FCP Report No. 33

FINITE ELEMENT SIMULATION OF THE MICROSTRUCTURE OF GRAY CAST IRON

by

Edward S. Russell
Department of Mechanical and Industrial Engineering

A two-dimensional finite element model was constructed in which the microstructure of gray cast iron was represented as an array of graphite flakes in a steel matrix. These flakes were allowed to open in tension but to resist compression. The computer program which was used has cyclic plasticity capabilities and can simulate crack growth.

The model was shown to simulate the tensile, constant amplitude cyclic, and variable amplitude cyclic responses of gray iron well enough to include all the characteristic features of gray iron behavior. The potential was demonstrated for using the model to investigate the effects of variations in microstructure on mechanical behavior of gray iron.

A Report of the
FRACTURE CONTROL PROGRAM
College of Engineering, University of Illinois
Urbana, Illinois 61801

December, 1979

ACKNOWLEDGMENT

This investigation was funded by the Fracture Control Program at the University of Illinois. Tests were conducted in the Materials Engineering Research Laboratory.

I thank my advisor, Professor Darrell F. Socie, for his help in all phases of the project and for his measured supervision which has encouraged independent thinking as well as self-discipline, adding to my professional growth. Professor JoDean Morrow has done much to inspire my technical pursuits and I am grateful to him to many enriching discussions, technical and otherwise.

Mr. Jack W. Knott of the Digital Computation Laboratory was of great service in helping me to acquire the enormous computer space and time capabilities required to run the program. Messrs. Eliot Zaiken and Victor Osowski are thanked for drafting some of the figures and June Kempka for typing the manuscript.

TABLE OF CONTENTS

1. OBJECTIVE

In the last ten years, techniques have been developed to predict the fatigue life of a wrought metal component or structure under service loading [1]. These methods employ three types of input: material properties, component geometry, and strain history under service conditions. The analysis requires a knowledge of the cyclic stress-strain behavior of the material so that a stress history can be obtained from a strain history. However, the models for describing cyclic behavior used in the present successful life prediction techniques are limited to metals which have a symmetric cyclic response, so that these methods cannot be extended to gray cast iron, which does not possess such symmetry. Thus, development of a model to describe cyclic behavior in gray iron is a necessary prelude to applying present life prediction techniques to this material.

The asymmetric cyclic behavior of gray iron is a result of its inhomogeneous microstructure, which consists of graphite flakes in a steel matrix. It has been shown [2] that the effect of these flakes on the tensile behavior of gray iron can be simulated with steel plates into which arrays of slots have been machined. The present paper shows that a finite element model analogous to the slotted plate model can simulate not only the tensile behavior of gray iron but also its cyclic behavior under constant and variable amplitude loading. The capability of the model to investigate the effects of various microstructural parameters on mechanical behavior is also demonstrated.

2. BACKGROUND

Mitchell [3] developed a technique to predict the fatigue life of cast irons and steels and high hardness wrought steels. These materials are similar in that they contain microdiscontinuities which, acting as internal notches, reduce fatigue resistance and mechanical properties in general.

Gray cast iron is a particularly troublesome material, however. While the graphite nodules in nodular iron, for instance, can be assumed to be spheres and a microstructure-based description of mechanical behavior obtained, gray iron has no such geometric regularity in its microstructure. It has, on the other hand, a labyrinth of graphite flakes grouped in colonies, each of which forms the nucleus of a eutectic cell [4].

The extent of the colonies can result in a range of flake distributions, from a uniform distribution throughout the cell structure to distinct colonies within each cell. The ASTM A-247 designation is a measure of flake size, shape, and distribution [5]. A uniform distribution of randomly distributed flakes in a homogeneous matrix was assumed for the present work; this is ASTM Type A, shown in Fig. 1. The role of the eutectic cell boundaries was neglected.

This microstructure dominates mechanical behavior. The flakes are in the form of free graphite, a weak substance with a strength on the order of 1,000 to 3,000 psi [6]. Deformation of the flakes themselves is believed to be predominantly a volume increase due to void formation [7]. Plastic deformation in the steel matrix begins upon the first application of a tensile stress, due to the high stress concentration

at the flake tips. As the load increases, the zone of plasticity increases in size, manifesting itself in the characteristic non-linear stress-strain response of gray iron, shown in Fig. 2. The non-recoverable strain (the net strain upon unloading) is a sum of both plastic strain in the matrix and void formation in the flakes [7].

Since the flakes cannot transmit a tensile load and have sharp tips, they can be regarded in every sense as cracks. This leads to two factors governing the mechanical behavior of gray iron. First, as in any cracked member, the elastic modulus and all strength properties are greater in compression than in tension. Second, the cyclic response of gray iron in strain control shows a continuously decreasing maximum stress, due to the growth of cracks out of flake tips throughout the specimen and the resulting continuous increases in compliance. This effect is depicted in Fig. 3. Since gray iron is from the beginning a cracked member, the study of its fatigue resistance should treat it as a crack propagation problem [9], albeit a complex and forbidding one.

3. FINITE ELEMENT MODEL

In 1929, Thum and Ude conducted a series of tests in which they subjected steel plates containing arrays of slots to tensile loading [2]. They showed not only that the load-displacement curves of such plates are similar to the stress-strain curve of gray cast iron, but that the longer the slots are, the lower is the elastic modulus, just as gray iron is more compliant with longer flakes. Their results are shown in Fig. 4.

A similar model of an array of slots was constructed for the present study using elastic-plastic finite elements. Many complexities of the problem can be examined using finite elements which could not be studied in the pre-computer era. The slots can be allowed to open in tension but to resist compressive loading, thus more accurately modeling the behavior of graphite flakes. Flake size, shape, and distribution can be varied to examine their effect on mechanical response of the model. The distribution and growth of plastic zones around flakes can be plotted.

The computer program used for this work solves a plane stress or plane strain problem using constant strain triangles. It has cyclic and plasticity capabilities and can simulate crack growth using bar elements [10]. For this work, it was modified to accommodate a model containing two different materials. The program is described in greater detail in APPENDIX A. APPENDIX B lists the input data required.

Several assumptions were made to reduce the complex nature of flakes to a model which could be used in the finite element analysis.

The steps in this idealization are depicted in Fig. 5. The first assumption, of course, is that the problem is a plane one. The second is that the flakes are arranged in a regular alternating array and are all oriented perpendicular to the loading direction. Then, taking advantage of symmetry about the longitudinal and transverse axes of a flake and imposing the appropriate boundary conditions, the model is reduced to one with three flake halves.

A typical finite element mesh is shown in Fig. 6, in which the flakes are demarcated by bold lines. Outside of these lines, the elements are given the properties, listed in Table 1, of SAE 9262 (high silicon) steel, which is comparable in hardness and composition to the matrix steel of a pearlite gray iron with a DPH 272 matrix hardness [11]. The asymmetric properties of the flakes are modeled by using bar elements which open when the net displacement across a flake is positive and which close when this displacement is negative, as illustrated in Fig. 7. In compression, these bar elements add a stiffness corresponding to the elastic modulus of graphite. The modulus of graphite brick is 1.4×10^6 psi [6] but a smaller value, 10^6 psi, was used here since the free graphite which makes up the flakes was not thought to have the strength of a commercial graphite.

The boundary conditions imposed are shown in Fig. 8. They prohibit vertical displacements along the bottom edge and horizontal displacements along the right-hand edge. Uneven displacements on the upper, loaded edge were corrected by adjusting the load distribution there to achieve a constant displacement. The load distribution applied is shown in Fig. 9. No constraints were placed on the left-hand edge since

restricting horizontal displacements there would stiffen the model by resisting Poisson contraction. Since this edge was stress-free, errors were introduced due to its distortion, but the location in the model where strain was measured (to be described shortly) was assumed to be far enough from the distorted left-hand edge that, by Saint-Venant's principle, these distortions did not affect the strain measurements.

Strain in the model was defined as the average displacement of the nodes, on a horizontal line extending from the tip of the middle flake to the right-hand edge, divided by the y-coordinate of this line, as shown in Fig. 10. This line should be a line of symmetry and was, in fact, observed to displace uniformly.

Micrographs of plane sections of a gray iron, similar to that from which the matrix properties were determined, were examined to obtain an estimate of the average separation distance between flake tips and the length-width ratio of a representative flake. Several meshes were then constructed of different flake separations; their stress-strain responses are shown in Fig. 11, along with the curve for a gray iron. These results were then plotted in a different manner in Fig. 12, in which each curve represents the stress at a given strain as a function of a/s, the ratio of flake length to flake separation. The intercepts with the stress axis correspond to points from the stress-strain curve of the matrix steel, which has no flakes and thus has an a/s ratio of zero. Lines are drawn, from the stress axis to each curve and then down to the a/s axis, corresponding to points on the gray iron stress-strain curve. For example, a strain of 0.003 in this particular gray iron yields a stress of 28.5 ksi. The construction on the figure shows that

at this point on the stress-strain curve, the iron has an effective a/s ratio of 1.4. Clearly, if the stress-strain response were modeled exactly, all the vertical lines would coincide. A model, with an a/s value in the range of the effective a/s for this iron, was constructed for further studies. It is easily seen that another grade of iron would plot differently on these curves and thus would have a different effective a/s ratio.

The initial estimate of a/s, based on microscopic examinations, was 5. The discrepancy between this number and the effective a/s values in Fig. 12 means that gray iron behaves as if the mean flake separation were larger than it appears to be under a microscope. Two possible explanations for this are as follows: First, since the flakes are randomly oriented, a certain fraction of them are aligned along the direction of loading and thus have little effect on deformation of the matrix. Second, the flakes are actually three-dimensional and, as such, have a lower stress concentration than a plane model would predict [9].

4. RESULTS

A comparison of the monotonic response of the finite element model to that of cast iron is shown in Fig. 13. While the curve was not simulated exactly, the model exhibits the continually decreasing slope characteristic of gray iron and thus is qualitatively correct. The model could have been "fine tuned" in several ways to more closely match the response of a particular iron, but doing so was not the purpose of this study.

In Fig. 14, a comparison of the stress-controlled cyclic response of the model to that of a specimen shows remarkably similar behavior. The higher modulus in compression is evident, as is the inflection of the curve on the compressive reversal of the loop. Figure 15 shows the response of the model under several cycles in strain control. A comparison with Fig. 3 reveals the similarity in behavior between model and specimen.

The reversed curvature on the downward reversal of a gray iron hysteresis loop marks the region where flakes begin to close and thus to support compressive loads, stiffening the material. This region occurs at a compressive stress since the matrix has been deformed in tension; the resulting compressive residual stresses at the flake tips prevent closure upon unloading to zero. The same effects are seen in the model; crack closure loads, included in the program output, confirm that closure indeed occurs at compressive loads.

Two variable amplitude stress sequences, depicted in Fig. 16, were applied to the model and the response again exhibited all the characteristics shown by a gray iron specimen, as seen in Figs. 17 and 18.

Amplitudes for the model were selected to give the same width of the hysteresis loop as was exhibited by the specimen.

Two different microstructural parameters were varied and their effects on stress-strain behavior of the model examined. Since the finite element results are independent of the magnitude of dimensions in the mesh, these parameters were expressed as ratios. The first of these is the a/s ratio described earlier in discussion of the development of the model. By referring back to Figs. 11 and 12, it is seen that a small change in a/s has a large effect on stress-strain response. Figure 19 shows the effect of a/s on the initial elastic modulus.

The other parameter varied was a/r, the ratio of flake length to flake tip radius. In doing so, a/s was held constant, which may have led to the misleading results of Fig. 20. It appears that the sharper the flake tip, the stronger the material, which is opposite to the observed trend in cast iron [2]. This contradiction can be explained as follows: Since the separation was held constant while the flake width was varied, the percent area of graphite in the model was varied, as illustrated in Fig. 21, and it was the change in graphite area, not the tip radius variation, which primarily affected the stress-strain behavior. That is, the higher the percentage of graphite, the weaker the material. This, in order to investigate the effect of flake tip radius, the amount of graphite should be held constant.

Bar elements similar to those used to represent flakes were inserted in nodes to the left of the lower flake and were opened as the model cycled, simulating crack growth, as shown in Fig. 22. A crack with a length 4 percent of the flake length was opened on the third

reversal; the resulting cyclic response is shown in Fig. 23 next to a control response of the same loading without a crack. The difference, while slight, shows an increased compliance as a result of the presence of a crack, consistent with observed behavior.

Figure 24 is a plot of the plastic zones at stress increments of 10 ksi. By comparing the size of the plastic zone with the monotonic curve of Fig. 13, it is seen that large non-linearity in the curve begins when net section yielding begins, between 20 and 30 ksi.

5. CONCLUSIONS

The effect of graphite flakes on the monotonic and cyclic behavior of gray cast iron can be modeled using finite elements. The external response of the model developed here is qualitatively identical to the behavior of a gray iron specimen. Internal processes of the model, such as flake opening and closing, are also compatible with those in the gray iron microstructure.

The model presented here can be used to study the effects of variations in the microstructure on the mechanical behavior of gray iron. For example, results of this study suggest that the mean separation between flake tips in the direction of loading has a large effect on the stress-strain response of gray iron.

Development of a model such as this one requires some experimentation with different variables before actual behavior is qualitatively simulated. Further adjustments would be needed in order to copy the exact behavior of a particular iron. Some of these variables are flake separation, flake tip radius, graphite stiffness, and flake orientation to loading direction.

6. RECOMMENDATIONS

Future work should initially be directed toward refining the model to simulate more accurately the shape of the stress-strain curve of a particular iron. Then the same could be done for different types of iron, each time using the correct matrix properties and finding the mesh configuration necessary to simulate behavior. Correlations could then be developed between appropriate parameters describing the flake size, shape, and distribution in gray iron and the corresponding parameters in the model.

Additional variations in the mesh might prove to be instructive. A different flake arrangement, such as rows and columns rather than the present alternating array, could be tried. Flakes could be oriented at different angles to the direction of loading.

Further investigations of crack growth out of flake tips could prove to be a valuable aid in developing a fatigue life prediction technique for gray iron. This would involve determination of crack growth rates for cracks of different sizes, based on crack tip stress and strain distributions obtained from finite element results, and crack propagation properties of the matrix steel. These crack growth rates could then be combined with data from microstructural observations describing mean flake length and mean separation between flake tips along a potential crack path; the number of cycles for a crack of a given length to grow by linking flake tips could then be estimated. If the fatigue lives thus estimated were to compare favorably with experimental results, a sound basis for predicting fatigue lives in gray iron components would result.

Table 1 Properties of SAE 9262 Steel at 272 DPH, Pearlite Matrix [11]*

Modulus of Elasticity, E	30×10^3 ksi
Yield Strength, 0.2% S_y	66 ksi
Strain Hardening Exponent, n	0.22
Strength Coefficient, K	253 ksi
Poisson's Ratio, ν	0.22
Strain Hardening Limit	100 ksi

*Only those properties used in the model are listed.

Type A

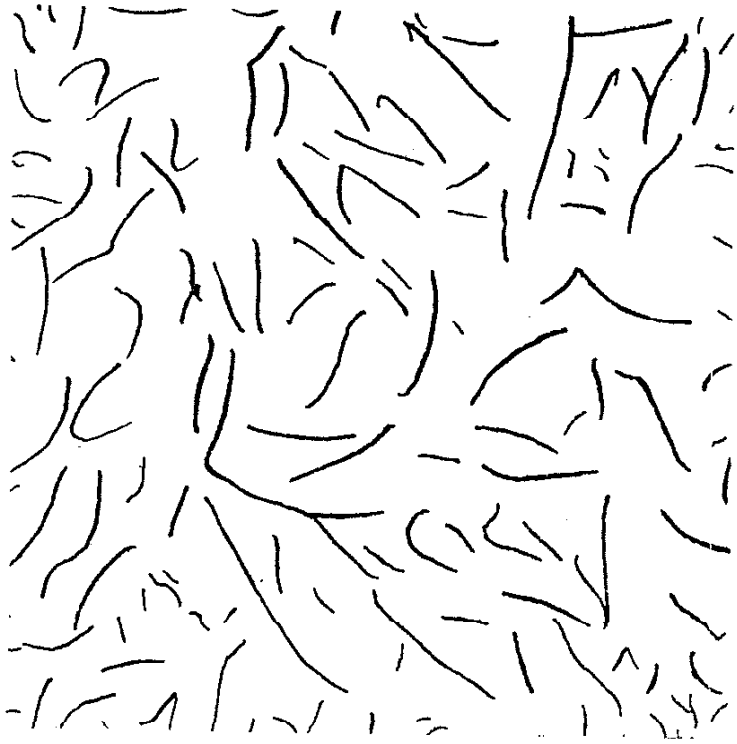

Uniform distribution,
random orientation

Figure 1. ASTM Type A Graphite [5]

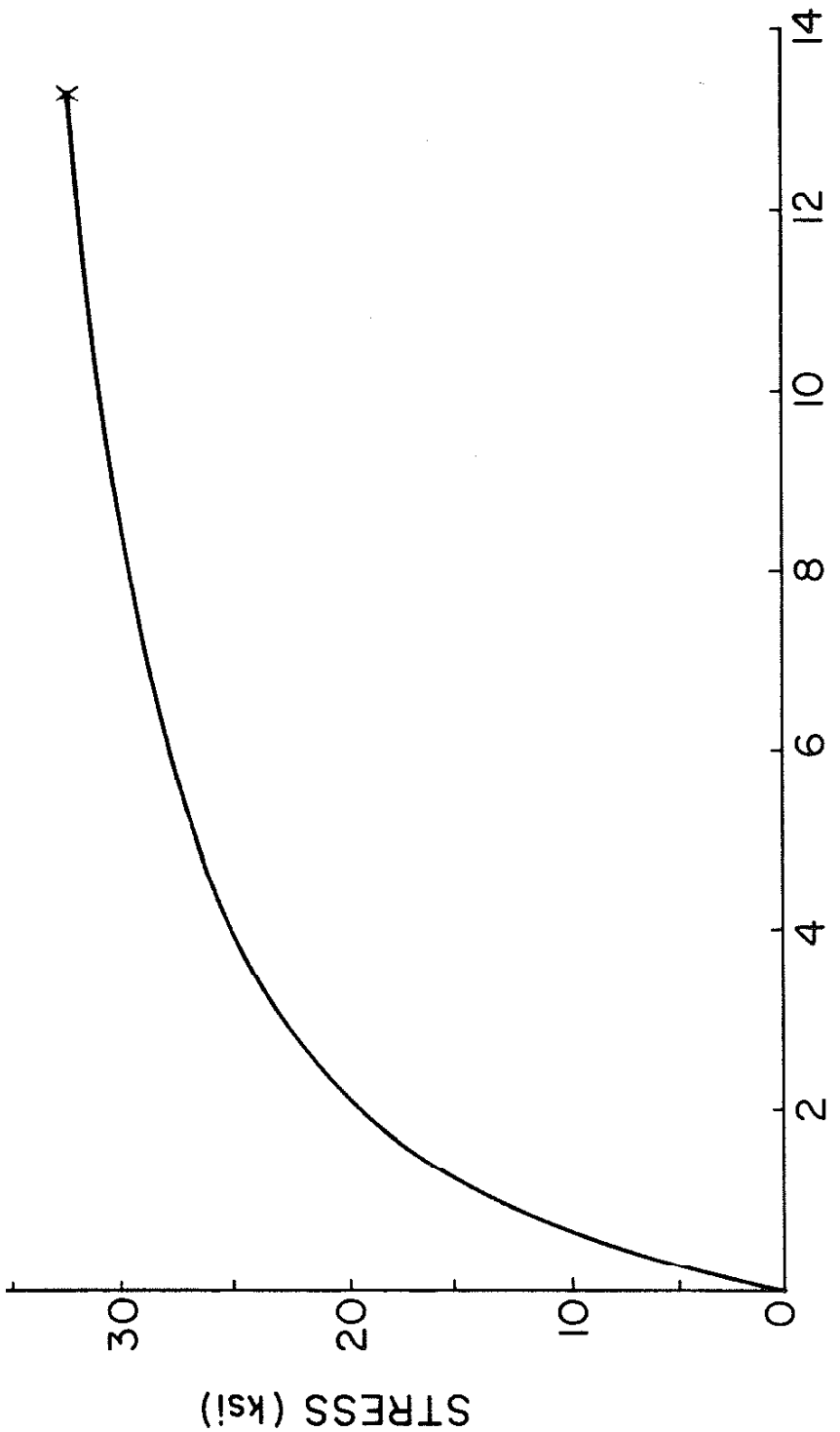

Figure 2. Tensile Curve of Gray Cast Iron

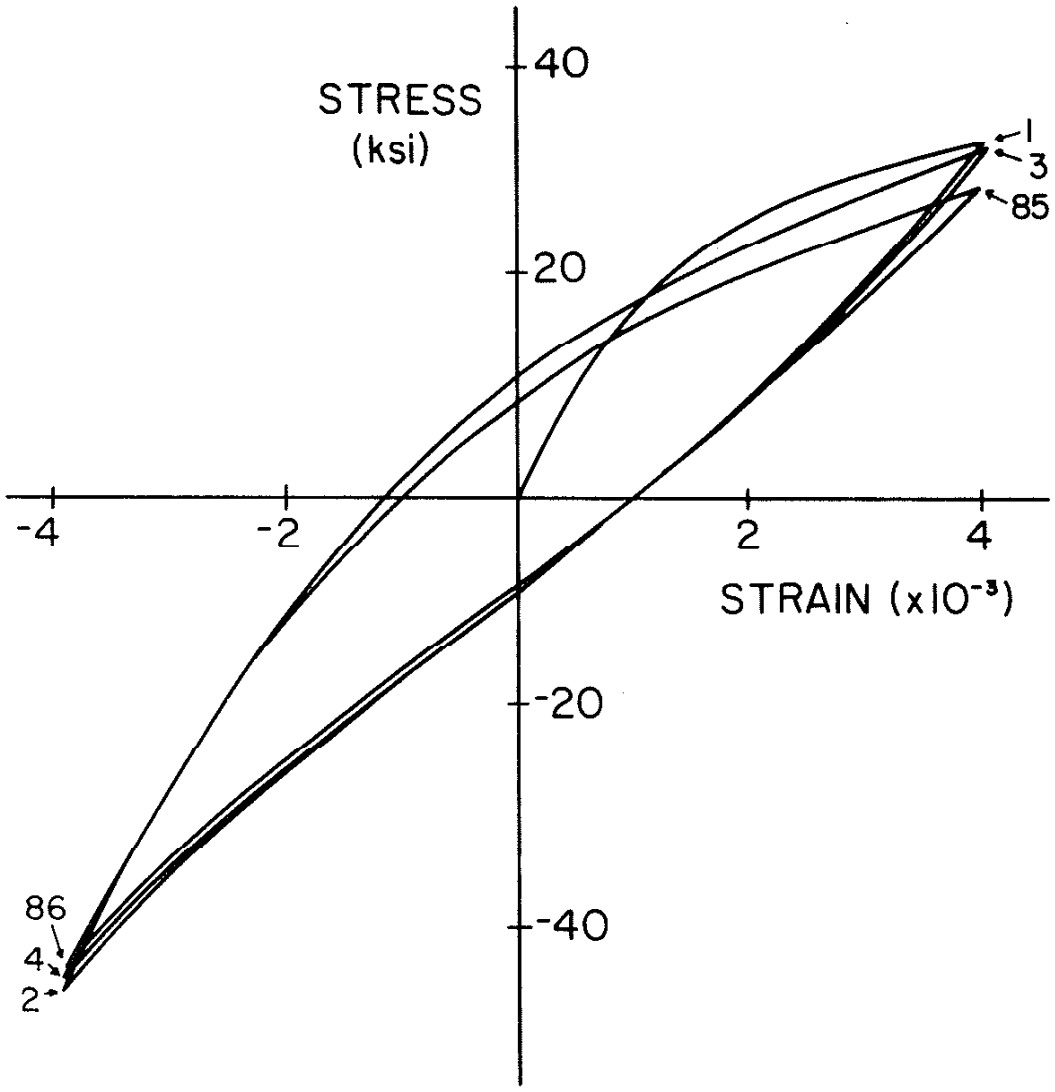

Figure 3. Cyclic Response of Gray Cast Iron in Strain Control showing Decrease of Maximum Load with Cycling

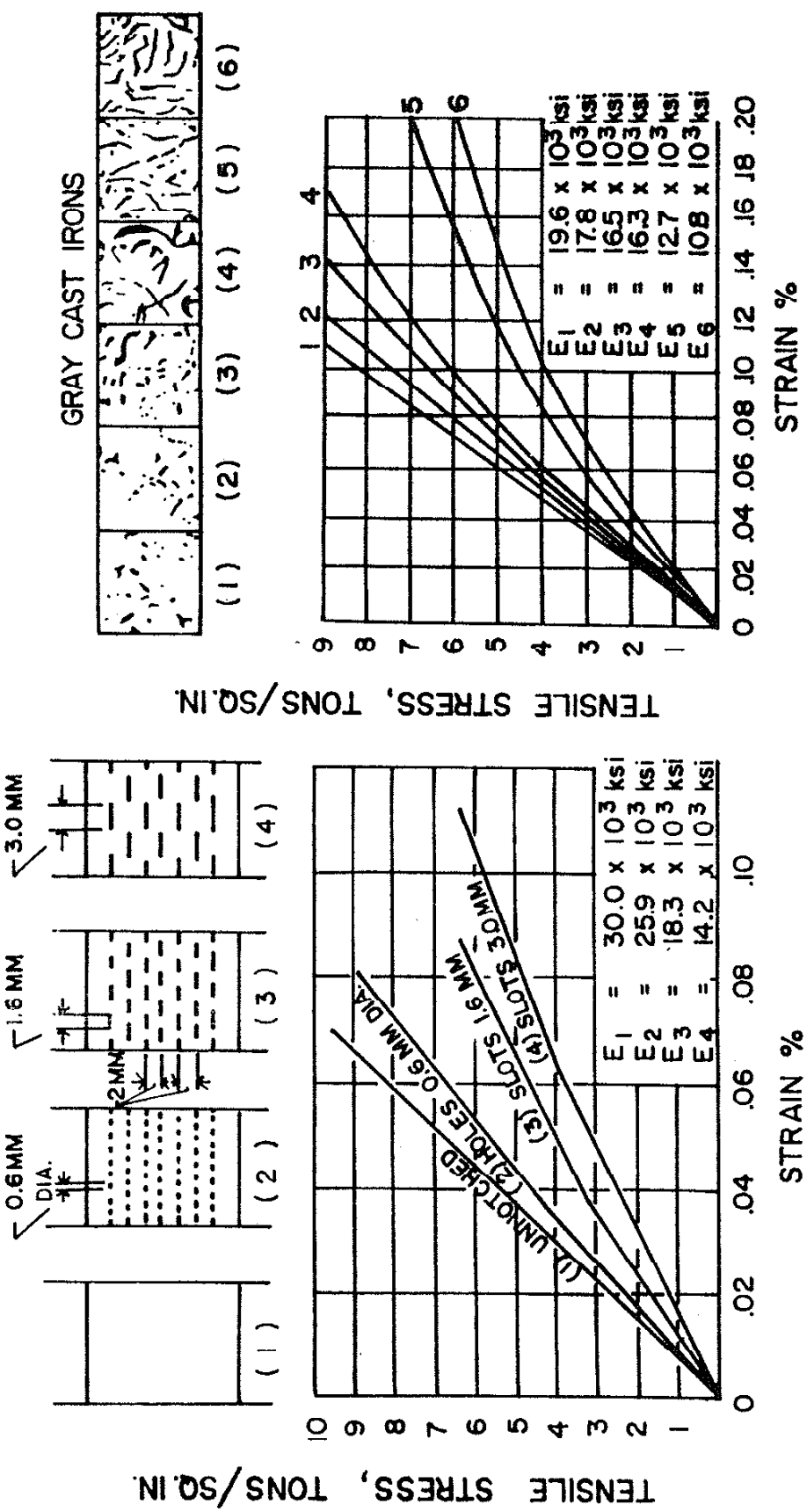

Figure 4. Stress-Strain Response of Model of Gray Cast Iron using Slotted Steel Plates (left) and Samples of Gray Cast Iron with Increasing Graphite Size (right) [2]

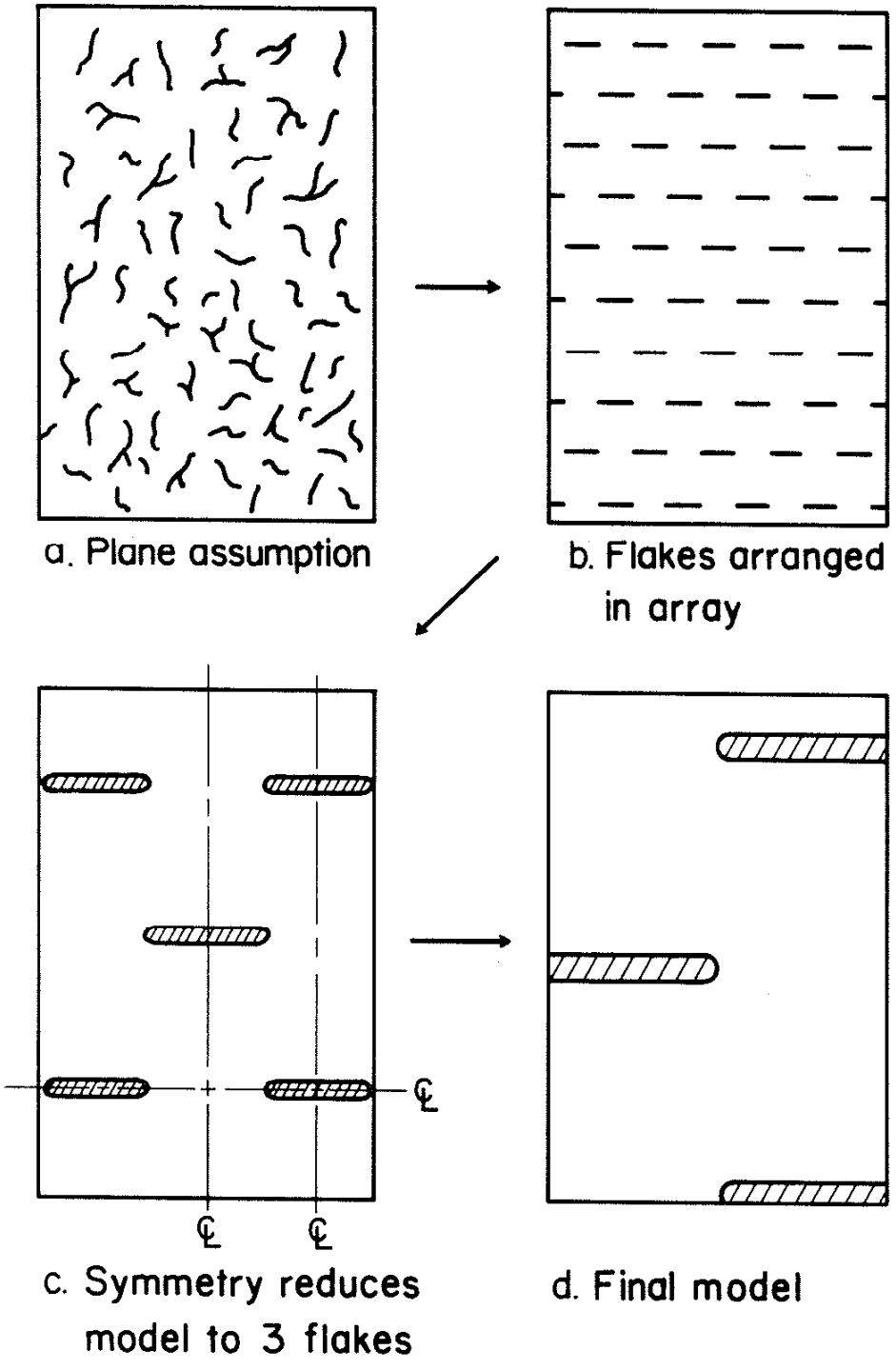

Figure 5. Assumptions Made in Developing Finite Element Mesh

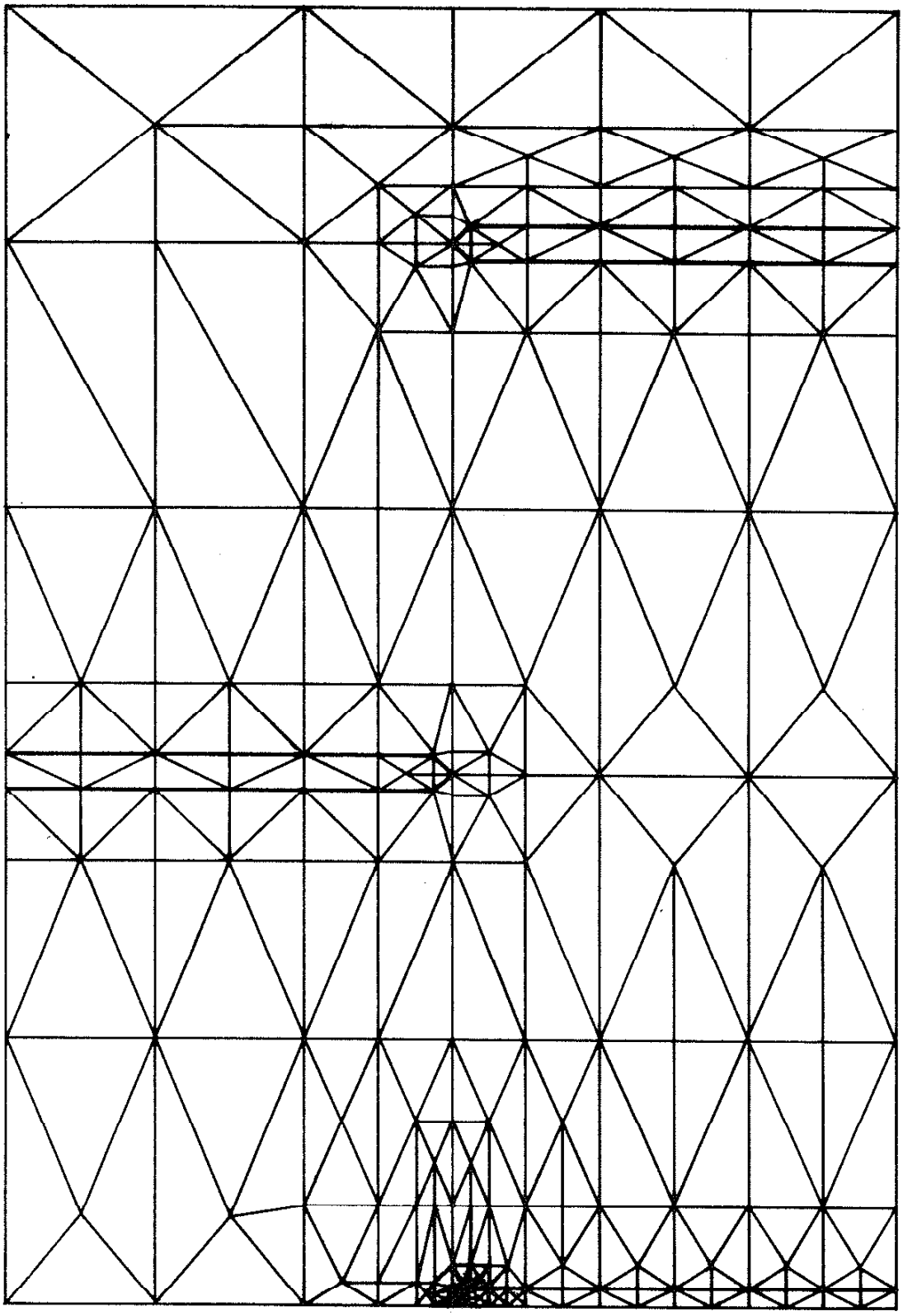

Figure 6. Finite Element Mesh

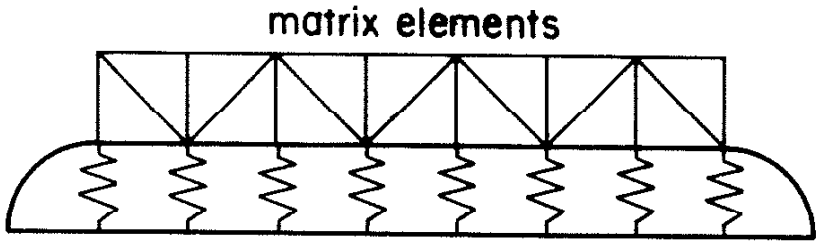

a. Undeformed flake (schematic)

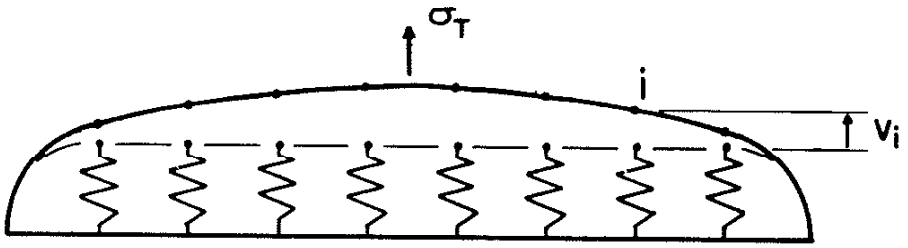

b. $v_i > 0 \rightarrow$ node i open

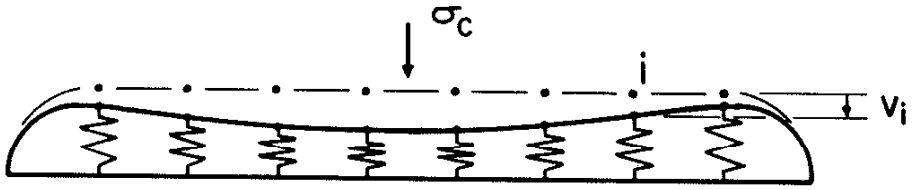

c. $v_i > 0 \rightarrow$ node i closed

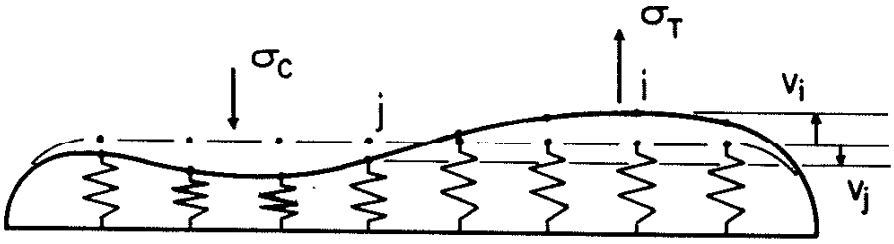

d. Node i open, node j closed

Figure 7. Representation of Graphite Flakes using Bar Elements

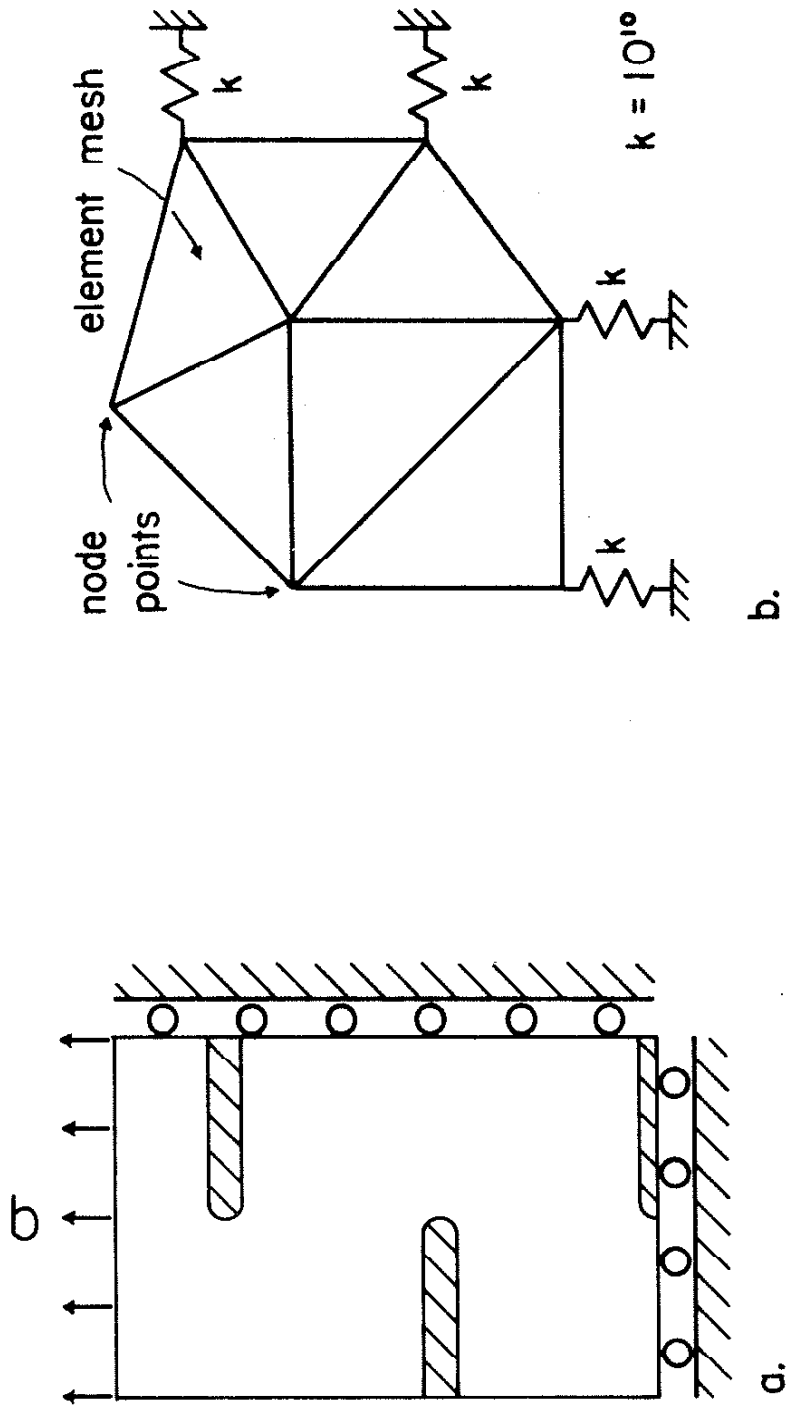

Figure 8. a. Boundary Conditions Imposed on Model
b. Representation of Rigid Boundary Conditions using Springs Attached to Fixed Nodes [10]

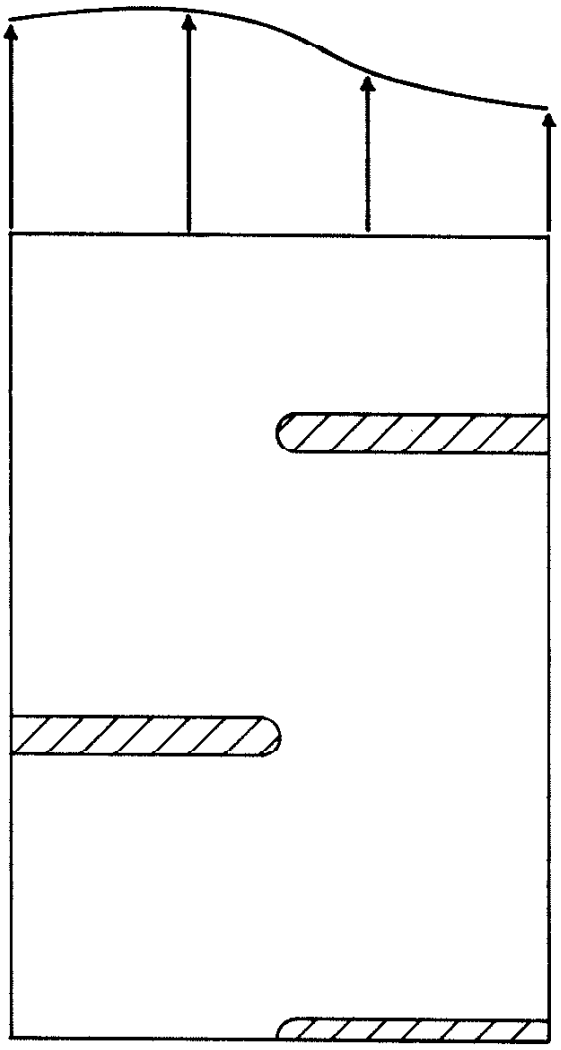

Figure 9. Load Distribution, along Top of Mesh, required to Enforce a Uniform Displacement

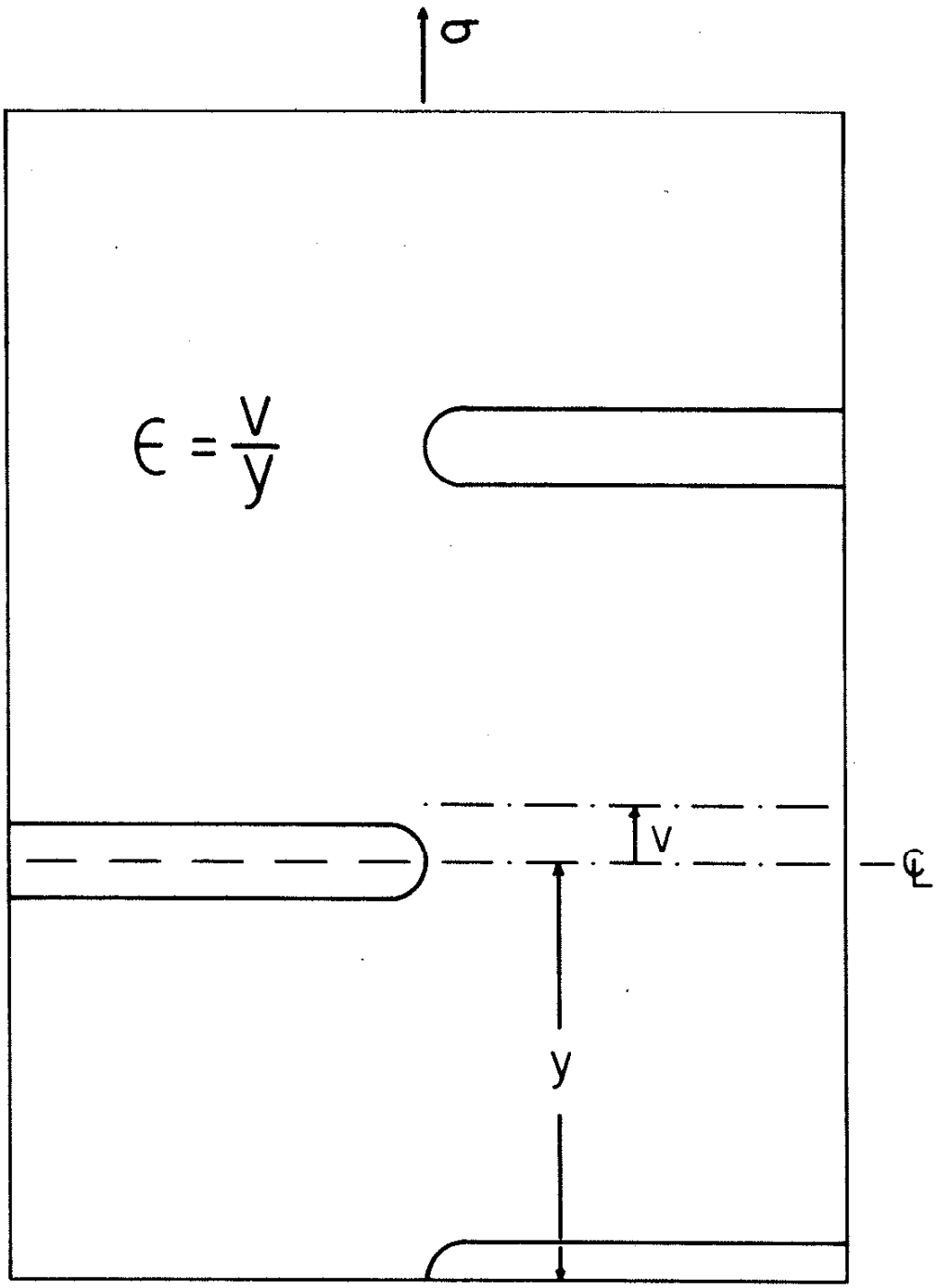

Figure 10. Definition of Strain in the Model

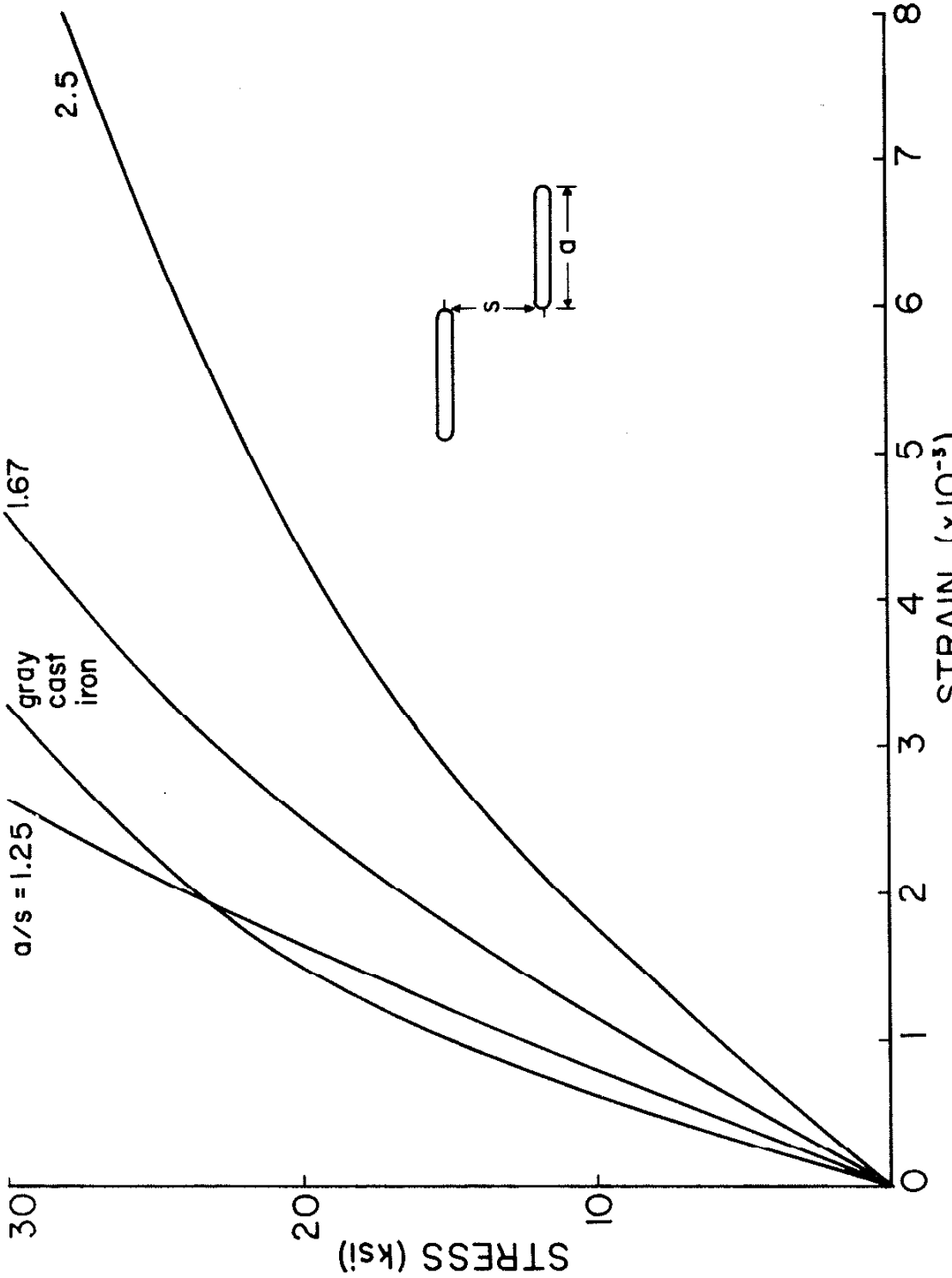

Figure 11. Stress-Strain Curves for Different Values of a/s.

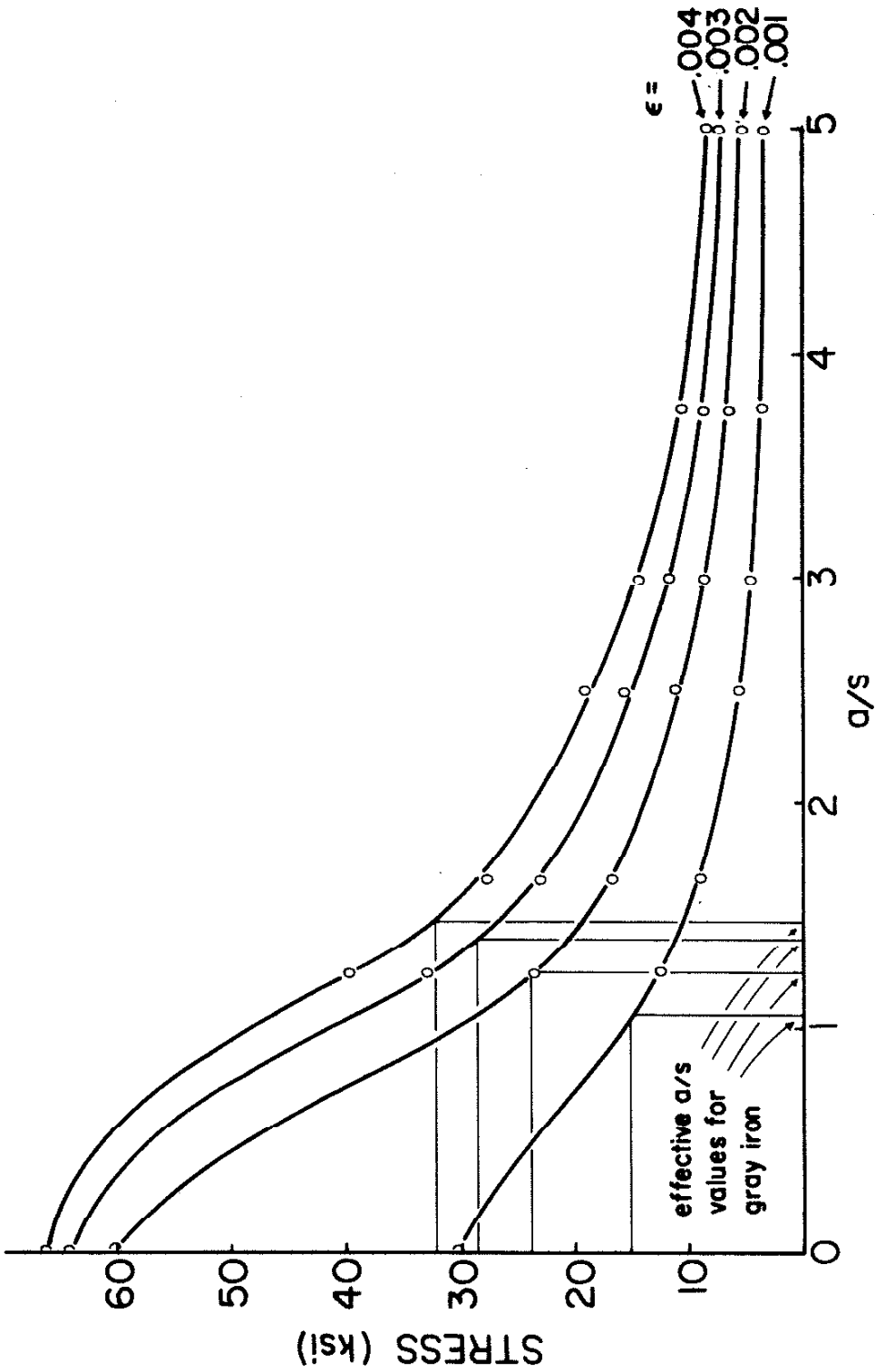

Figure 12. Stress at a Given Strain vs. a/s

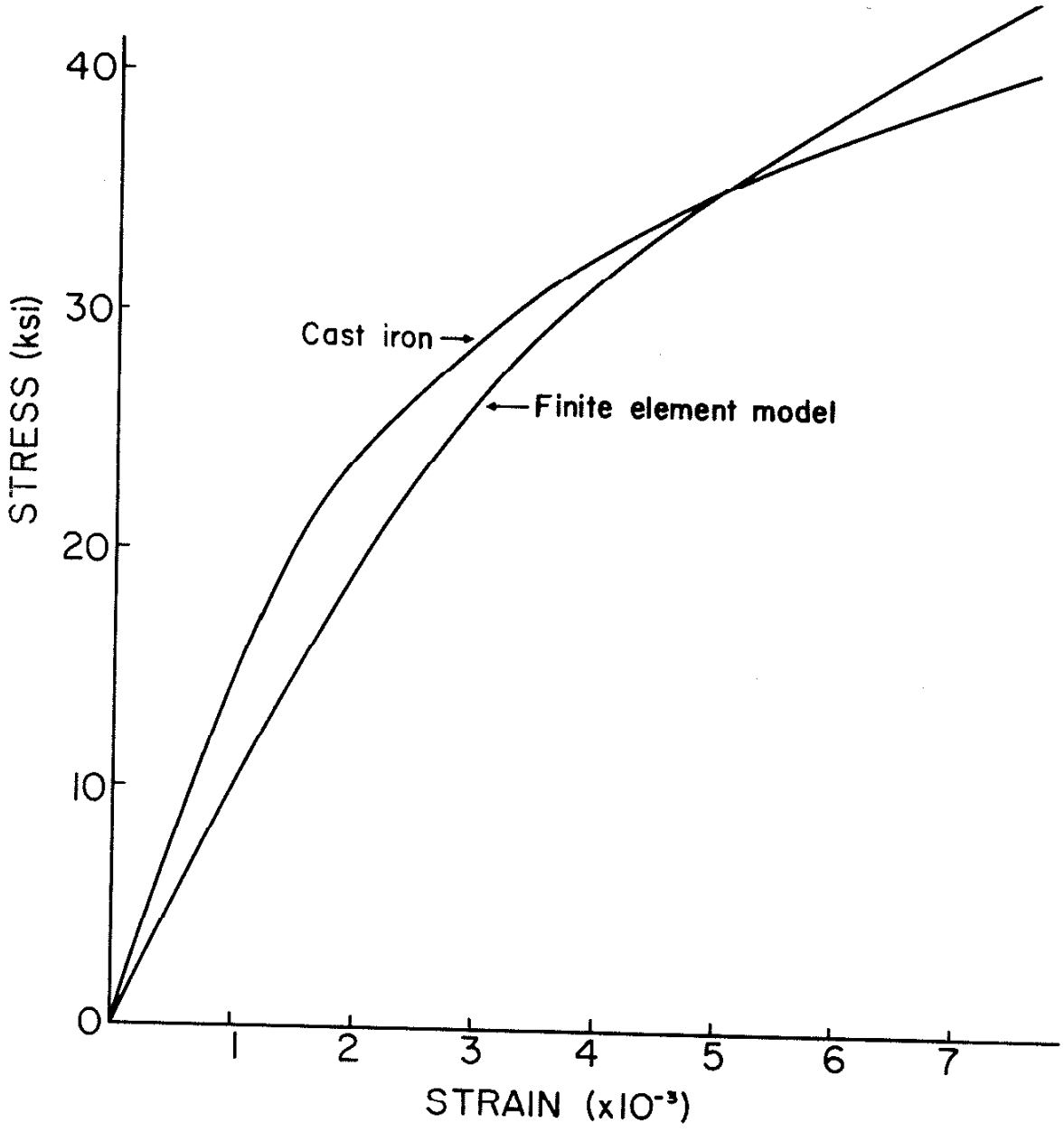

Figure 13. Tensile Stress-Strain Curves for the Model and a Gray Cast Iron Specimen

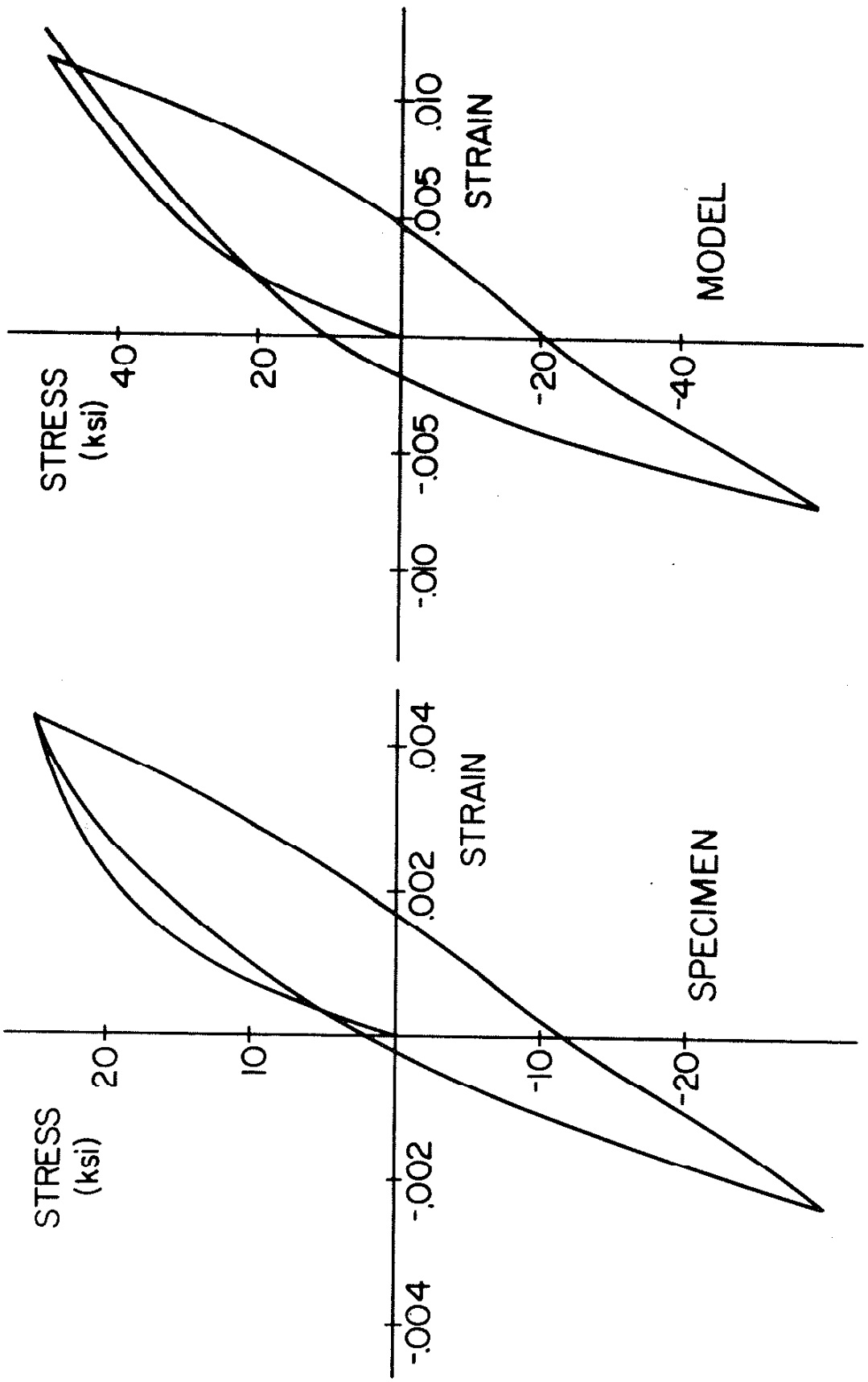

Figure 14. Cyclic Response of the Model and a Specimen in Stress Control

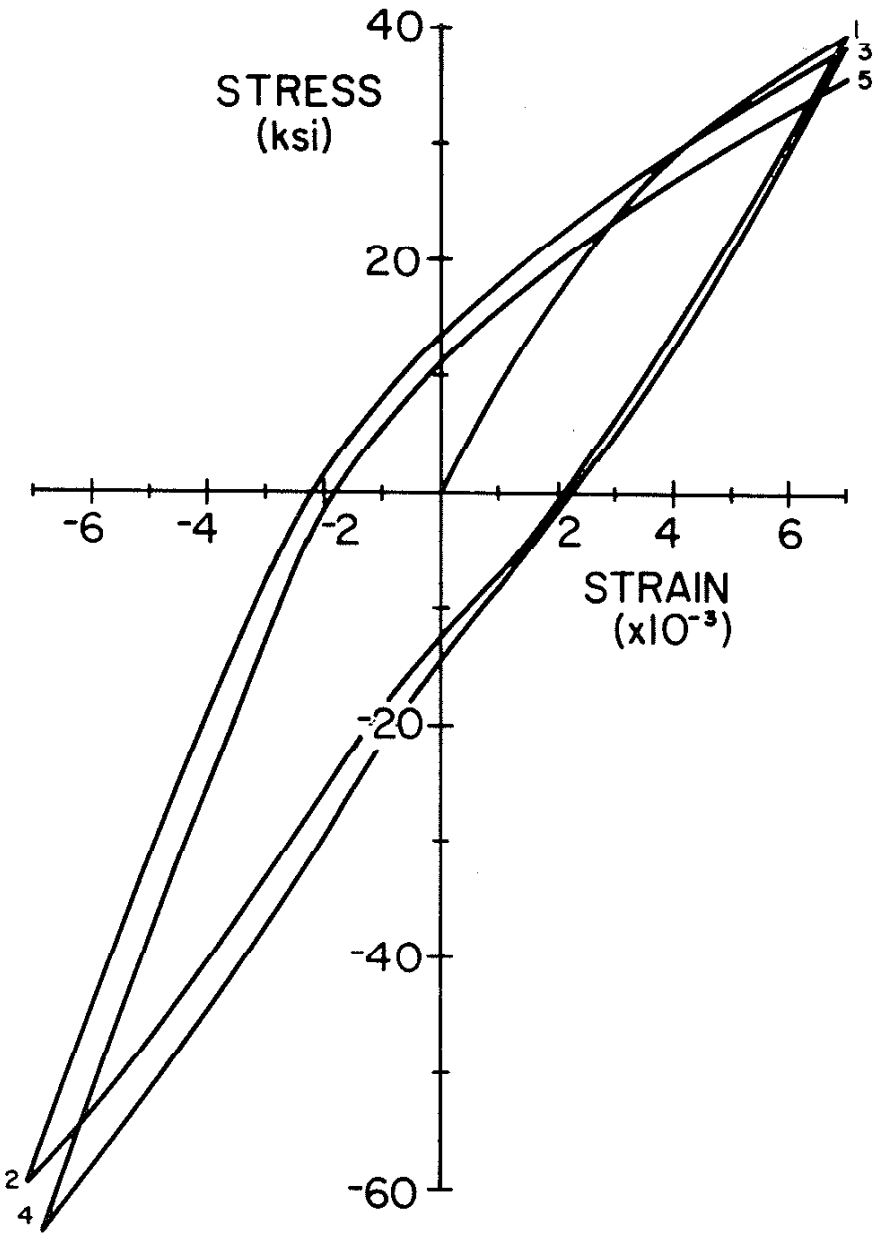

Figure 15. Cyclic Response of the Model in Strain Control

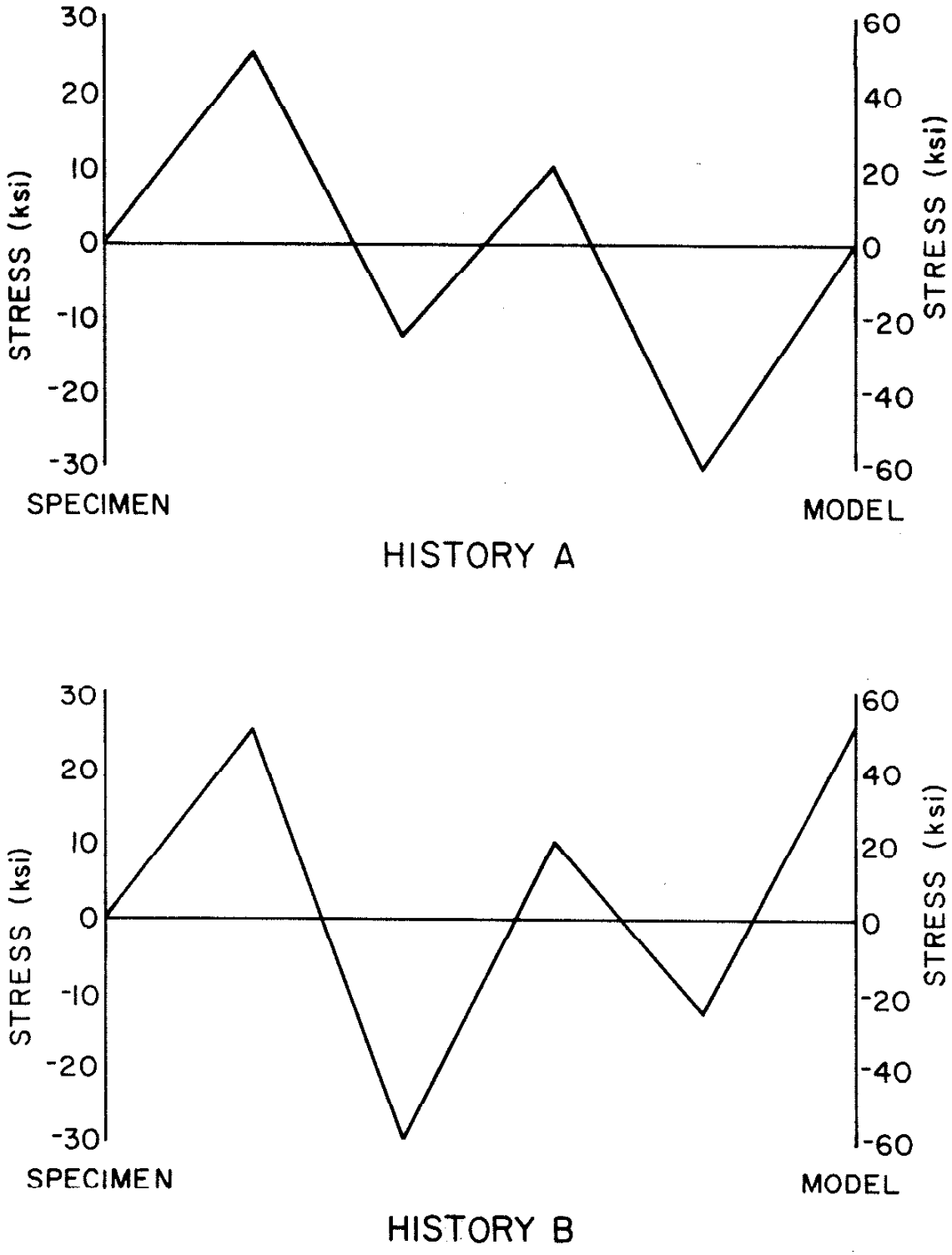

Figure 16. Variable Amplitude Loading Sequences applied to the Model and a Specimen

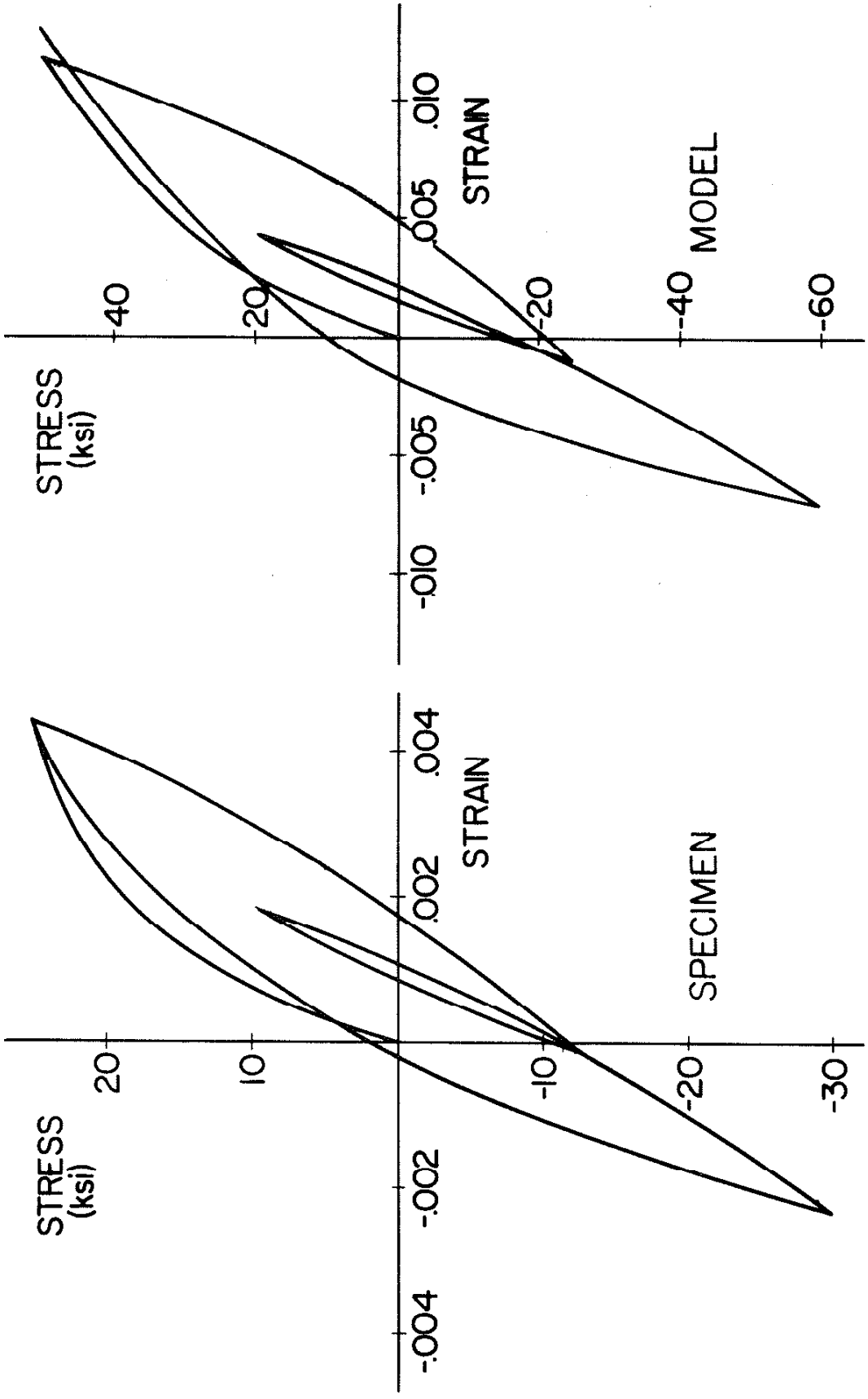

Figure 17. Response of a Specimen and the Model to Sequence A

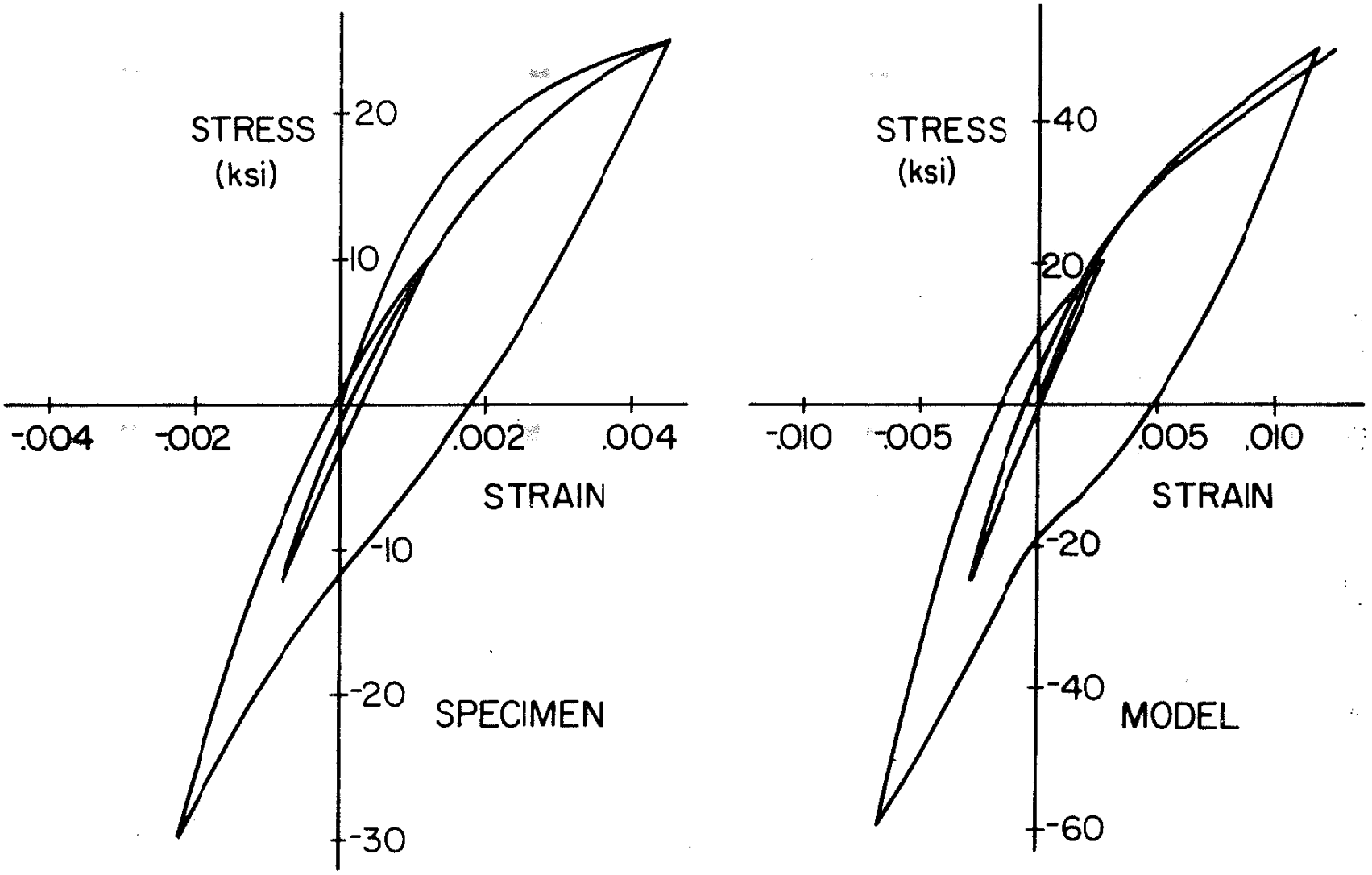

Figure 18. Response of a Specimen and the Model to Sequence B.

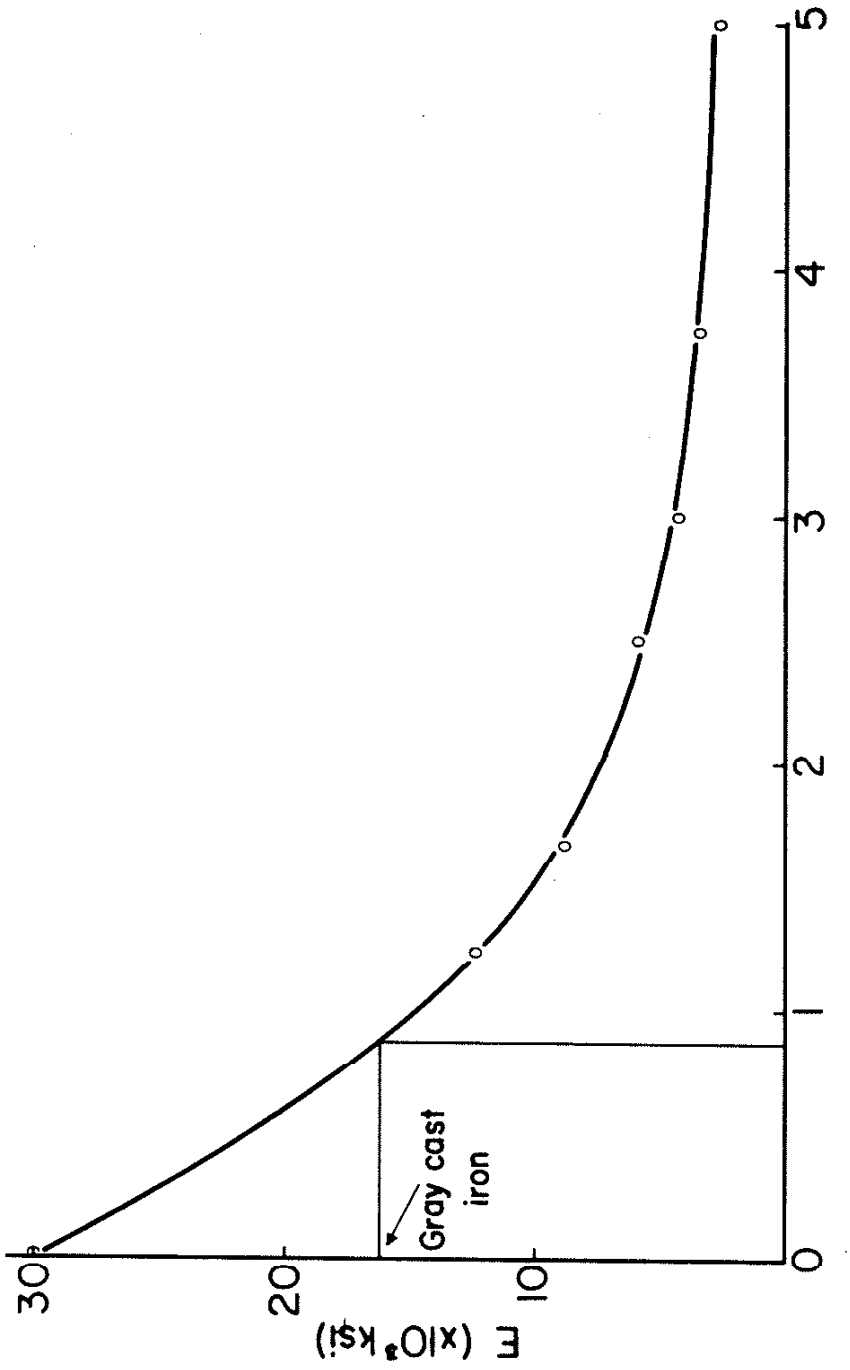

Figure 19. Elastic Modulus vs a/s

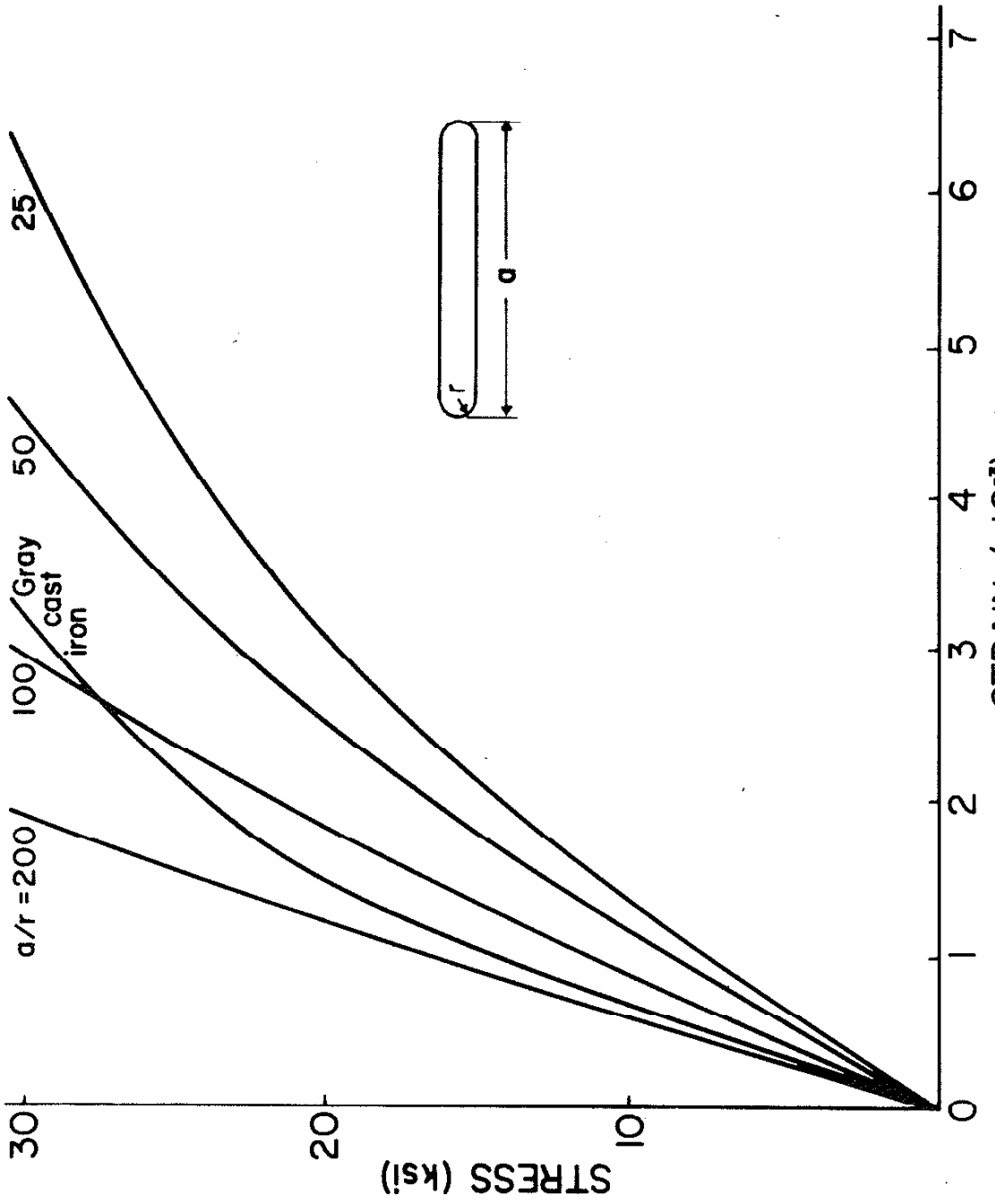

Figure 20. Stress-Strain Curves for Different Values of a/r

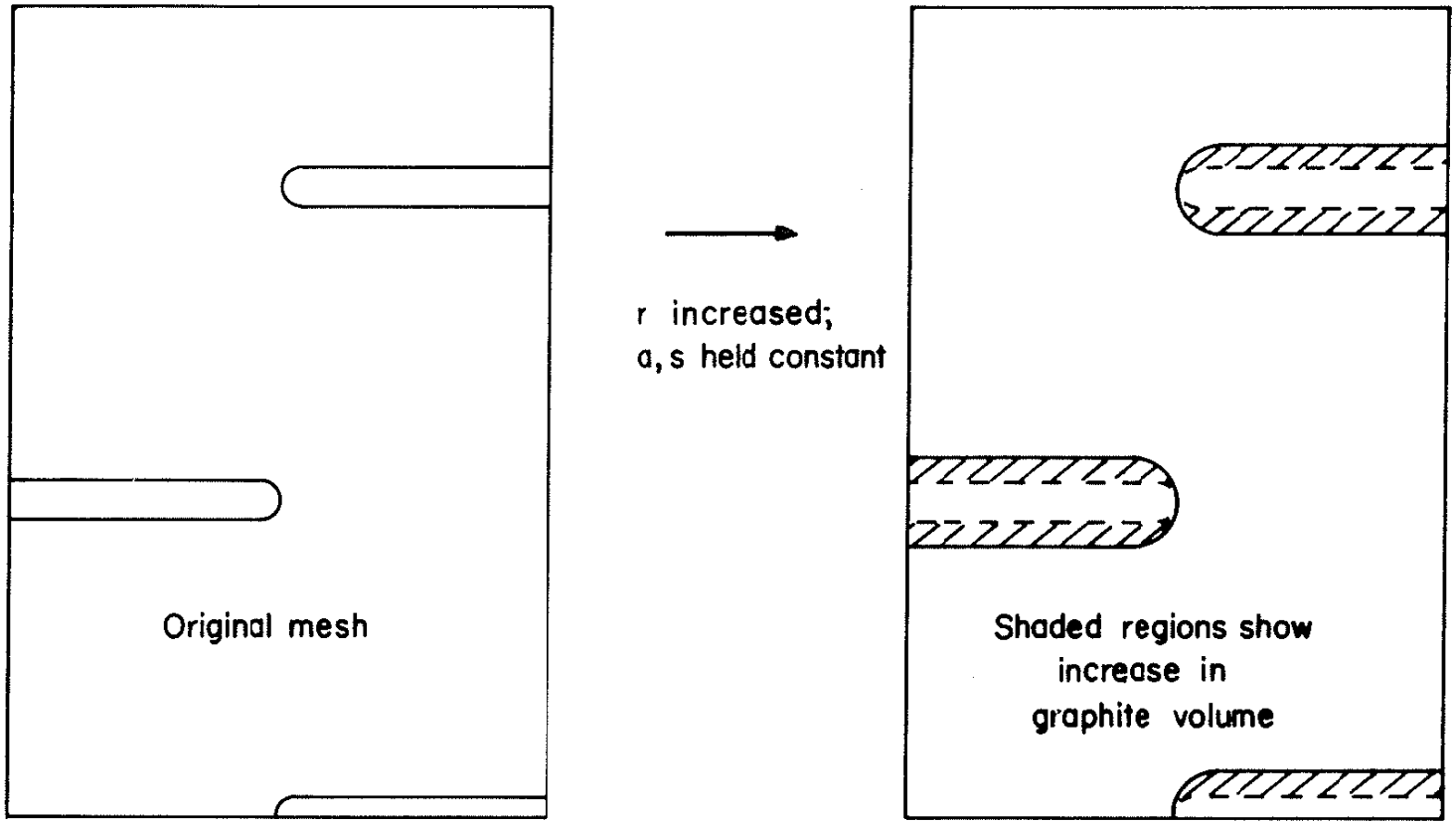

Figure 21. Increase in Graphite Volume as r is increased while a and s are held Constant.

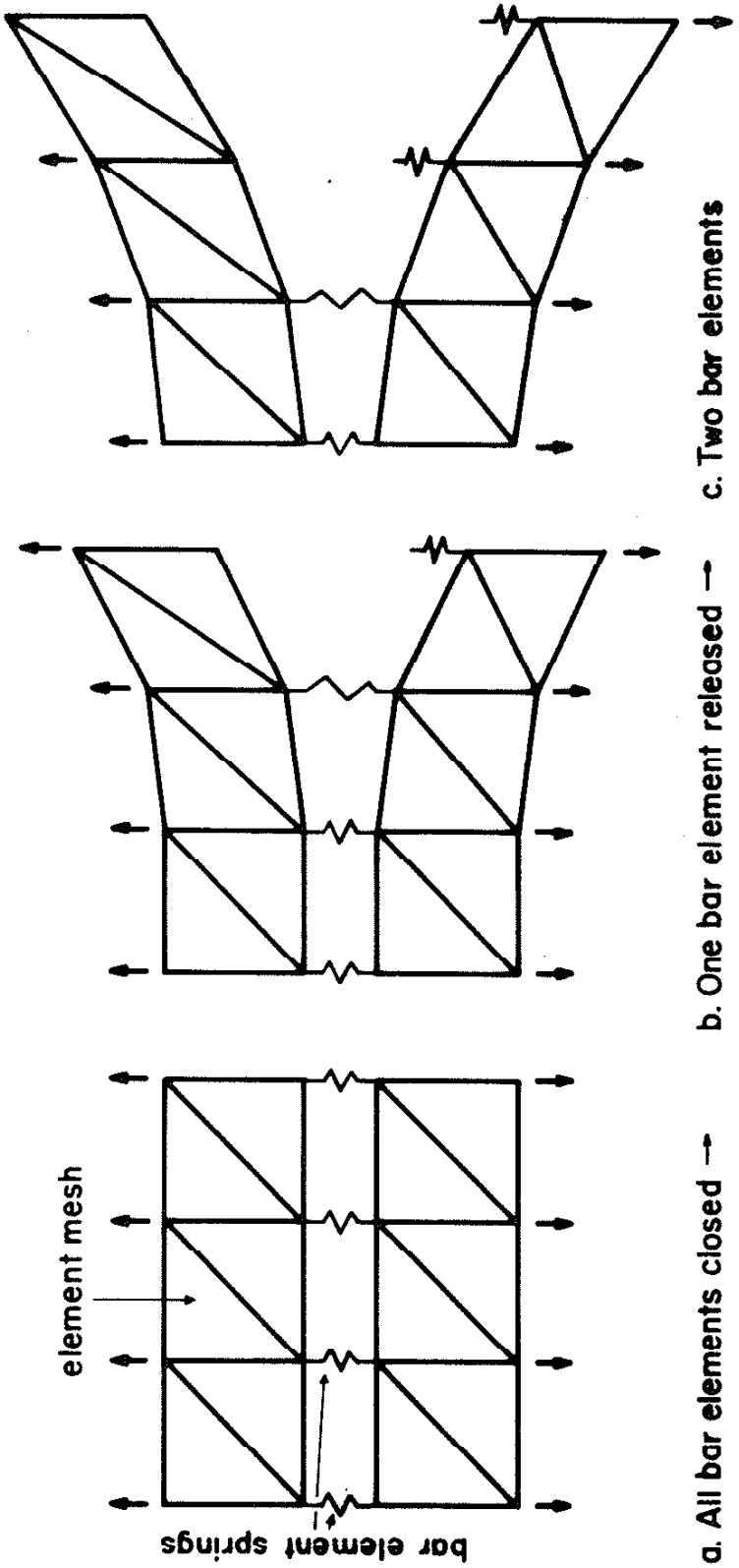

Figure 22. Representation of Crack Growth using Bar Elements

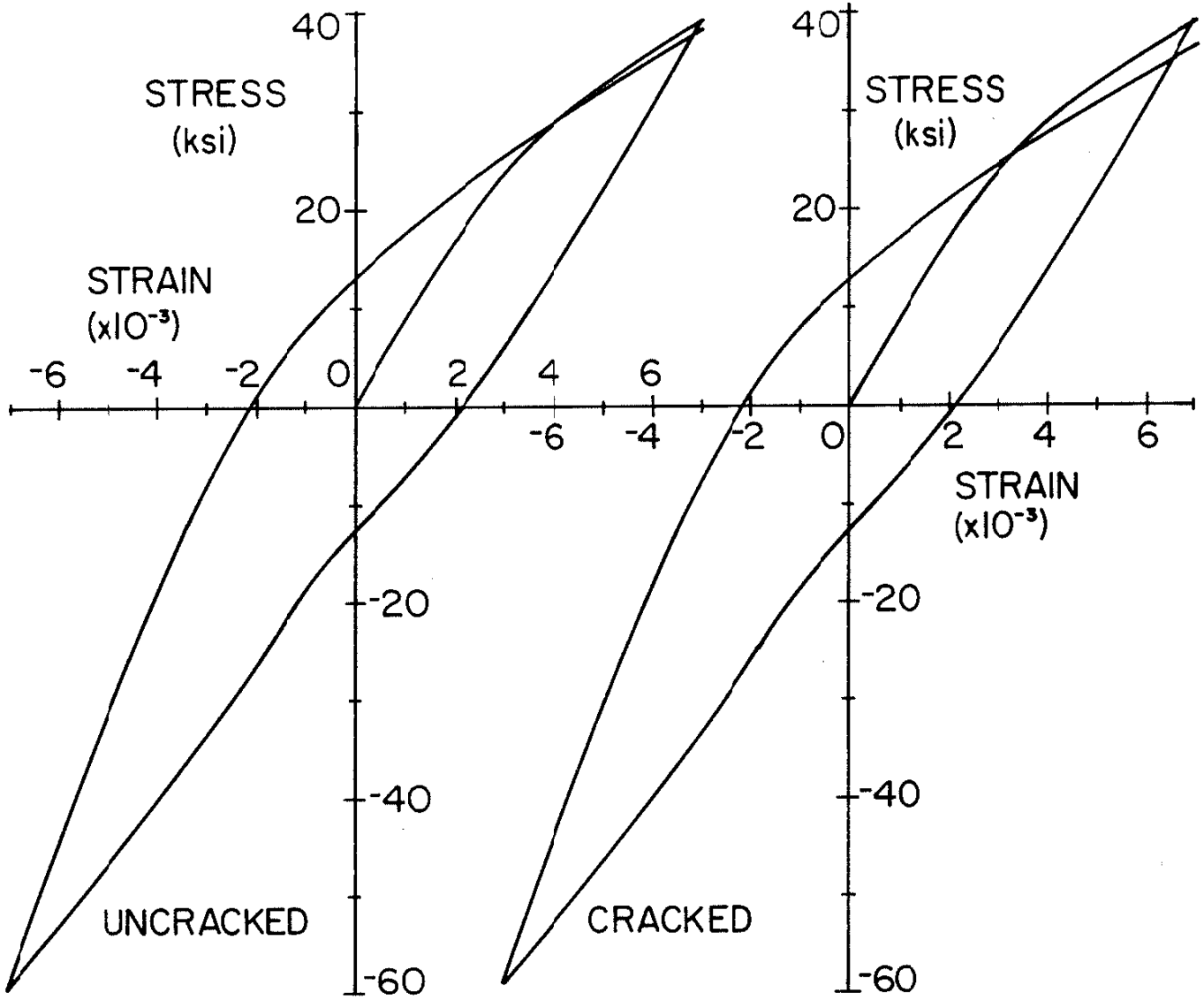

Figure 23. Control Response of Model without Crack Growth (left) and Response of Model with Crack Advance upon Third Reversal (right)

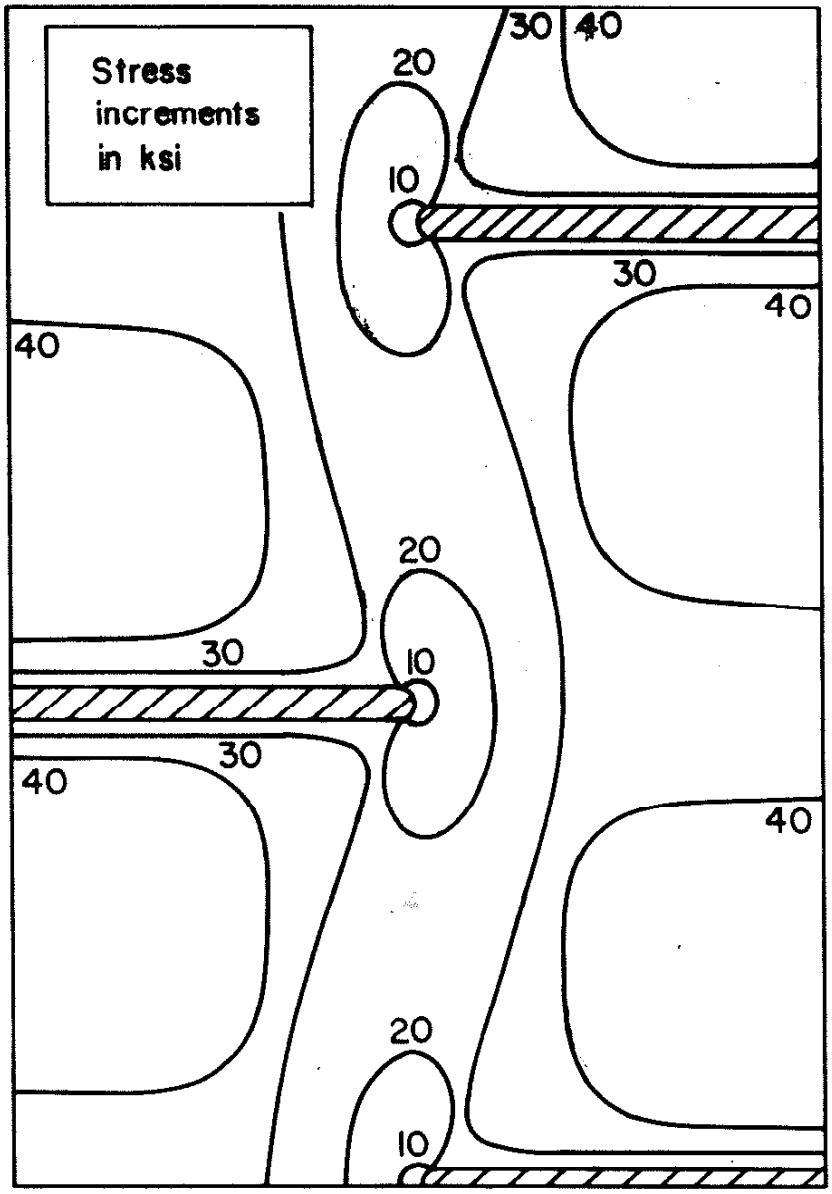

Figure 24. Growth of Plastic Zones as Model is Loaded.

REFERENCES

1. Wetzel. R. (ed.), Fatigue under Complex Loading: Analyses and Experiments, AE-6, The Society of Automotive Engineers, 1977.

2. Thum, A., and H. Ude, "Die Elastizitat und die Schwingungsfestigkeit des Gusseisens," Die Giesserei, Vol. 16, 31 May 1929, pp. 501-513, and Giesserei, Vol. 16, 14 June 1929, pp. 547-556.

3. Mitchell, M. R., "A Unified Predictive Technique for the Fatigue Resistance of Cast Ferrous-based Metals and High Hardness Wrought Steels," Fracture Control Program Report No. 23, University of Illinois at Urbana-Champaign, College of Engineering, Urbana, Ill., Sept. 1976.

4. Oldfield, W., "The Solidification of Hypo-Eutectic Gray Cast Iron," J. of the British Cast Iron Res. Assn., Vol. 8, No. 2, March 1960, pp. 177-192.

5. "Method of Evaluating the Microstructure of Graphite in Iron Castings," ASTM Designation: A247, Plate II (Graphite Flake Type Chart), American Society for Testing and Materials, 1916 Race St., Philadelphia, PA 19103.

6. Lynch, C., Handbook of Materials Science, Vol. III, CRC Press, Cleveland, 1975, p. 493.

7. Gilbert, G.N.J., "An Evaluation of the Stress-Strain Properties of Flake Graphite Cast Iron in Tension and Compression," J. of the British Cast Iron Res. Assn., Vol. 7, August 1959, pp. 745-789.

8. Gilbert, G.N.J., "Factors Relating to the Stress-Strain Properties of Cast Iron," J. of the British Cast Iron Res. Assn., Vol. 6, No. 11, April 1957, pp. 546-588.

9. Ikawa, K., and G. Ohira, "Fatigue Properties of Cast Iron in Relation to Graphite Structure," American Foundry Society, Cast Metals Res. J., Vol. 3, 1967, pp. 11-21.

10. Socie, D. F., "Estimating Fatigue Crack Initiation and Propagation Lives in Notched Plates under Variable Loading Histories," T&AM Report No. 417, Dept. of Theoretical and Applied Mechanics, University of Illinois at Urbana-Champaign, Urbana, Ill., 1977.

11. Mitchell, M. R., "Effects of Graphite Morphology, Matrix Hardness, and Structure on the Fatigue Resistance of Gray Cast Iron," SAE Report No. 750198, 24 February 1975.

12. Lamba, H. S., "Nonproportional Cyclic Plasticity," T&AM Report No. 413, Dept. of Theorerical and Applied Mechanics, University of Illinois at Urbana-Champaign, Urbana, Ill., 1977.

APPENDIX A

CYCLIC PLASTICITY FINITE ELEMENT PROGRAM: VERSION IV (CYPLAS-IV)

CYPLAS is a special purpose program originally designed to obtain an elastic-plastic stress solution to a crack problem using the displacement finite element method. It employs constant strain triangles in a two-dimensional mesh. Prager's kinematic hardening was used in the original version of the program, but the program has since been changed to use a modified Mroz hardening rule [12].

Limit plasticity was simulated by limiting the effective stress to a constant value at higher strain levels. Stepwise linearization was used to incorporate the effects of plasticity and variable boundary conditions. Unloading from the plastic state is treated as an elastic process. The response of any element follows the stress-strain curve during the initial loading and the hysteresis loop shape during cyclic loading.

The present version of the program, unlike the original, allows crack growth anywhere inside the mesh, instead of only on the periphery, a capability crucial to the present work. The other necessary alteration, performed by this author, was the addition of a multi-material capability, in which each element is given the properties of one out of a maximum of three materials. This modification has given the program the capability to handle other special problems, such as welded and case-carburized components. The interested reader may find details of the matrix relations, plasticity equations, and solution procedures used in the program in Ref. [10].

APPENDIX B

INPUT INSTRUCTIONS FOR CYPLAS-IV

1. Identification

   Cols. 1-72 Mesh Identification----------IDENT

2. Mesh Information

   Cols. 1-5 Number of Nodes----------NODES

   6-10 Number of Plastic Nodes----------NODEP

   11-15 Number of Elements----------NELEM

   16-20 Number of Plastic Elements----------NELEMP

   21-25 Number of Traction Loadings----------NSLC

   26-30 0 = Plane Stress,
   1 = Plane Strain----------ISST

   31-35 Number of Bar Elements----------NBELEM

3. Material Properties (one material per card)

   Cols. 1-15 Elastic Modulus----------E(I)

   16-25 Strength Coefficient----------CSC(I)

   26-35 Strain Hardening Exponent----------SME(I)

   36-45 Yield Strength ----------SYS(I)

   46-55 Poisson's Ratio----------PR(I)

   56-65 Strain Hardening Limit----------SHLIM(I)

   66-70 Material Number
   (= 0 for last material)----------NMAT

4. Node Information (one node per card)

   Cols. 1-5 Node Number----------M

   6-10 Code 0 = X-load, Y-Load----------KODE(M)
   1 = X-Disp, Y-Load
   2 = X-load, Y-Disp
   3 = X-Disp, Y-Disp

11-20 X Coordinate----------X(M)

21-30 Y Coordinate----------Y(M)

31-40 X Boundary Condition----------ULX(M)

41-50 Y Boundary Condition----------VLY(M)

5. Element Information (one element per card)

Cols. 1-5 Element Number----------M

6-10 Node 1----------IE(M,1)

11-15 Node 2----------IE(M,2)

16-20 Node 3----------IE(M,3)

21-25 Material Number----------IE(M,4)

6. Bar Element Information

Cols. 1-5 Bar Element Number----------M

6-10 Node 1----------NBAR(M,1)

11-15 Node 2----------NBAR(M,2)

16-20 Code 1 = X Spring----------NBAR(M,3)
2 = Y Spring
3 = X and Y Spring

7. Surface Traction Loading

Cols. 1-5 Node 1----------ISLC(M)

6-10 Node 2----------JSLC(M)

11-20 X Traction at Node 1----------SURTRX(M,1)

21-30 X Traction at Node 2----------SURTRX(M,2)

31-40 Y Traction at Node 1----------SURTRX(M,1)

41-50 Y Traction at Node 2----------SURTRX(M,2)

8. Output Instruction and Crack Advance

Cols. 1-10 Printing Increment Size----------AINC

11-15 Printing Code----------KKOUT
- 4 = Stresses and Strains for Specified Elements
- 3 = Strains
- 2 = Stresses
- 1 - Stresses and Strains
- 0 = Stresses, Strains, and Displacements
- -1 = Stresses and Strains in Plastic Elements
- -2 = Stresses in Plastic Elements
- -3 = Strains in Plastic Elements

16-20 Number of Crack Advance Nodes (optional)----------ICLOSE

9. Printing Elements (optional)

14I5 Format Sequential Elements for Printing----------JELEM(I)

10. Crack Advance Nodes (optional)

14I5 Format Sequential Nodes for Crack Advance----------NOPEN(I,1), I = 1, ICLOSE

11. Initial Loading Data

Cols. 1-10 Maximum Load----------FLOAD

11-20 Loading Increment----------DLOAD

12. Cyclic Loading Data

Cols. 1-10 Load----------FLOAD

11-20 Load Increment (optional)----------DLOAD

21-30 Printing Increment (optional)--------AINC

31-35 Printing Code (optional)----------KKOUT

36-40 Nodes for Crack Advance (optional)----------IOPEN

41-45 Number of New Surface Tractions (optional)----------NSLC

13. New Surface Traction Loading (optional)

Same as Card No. 7.